Influence of Inhomogeneous Magnetic Field on Dynamic Behavior of Vortex–Antivortex Chains in the Superconductor/Ferromagnet Bilayer Structures

Y. Zhong[a], S. Du[a], S. Yao[a], L. Peng[a,*], J. Chen[a], L. Sang[b], J. Lin[a] and X. Liu[a]

[a] *Department of Physics, Shanghai University of Electric Power, Shanghai 200090, China*
[b] *Shanghai Key Laboratory of High Temperature Superconductors, Physics Department, Shanghai University, 99 Shangda Road, Shanghai 200444, China*

Received: 28.12.2022 & Accepted: 26.04.2023

Doi: 10.12693/APhysPolA.144.7 *e-mail: plpeng@shiep.edu.cn

Using a finite element method to numerically solve the time-dependent Ginzburg–Landau equations, we studied the influence of an inhomogeneous magnetic field on the dynamic behavior of vortex–antivortex chains in the superconductor/ferromagnet bilayer structures. Our results show that the coupling effect of superconductor/ferromagnet structures manifests as the vortex–antivortex pairs interaction. The coupling effect increases with the increasing level of inhomogeneity of the magnetic field. The periodic motion of the vortex–antivortex chains leads to the periodic oscillations of the magnetization and superconducting current in the superconductor film. The frequency of oscillations is adjusted by the inhomogeneous magnetic field and the external driving current.

topics: superconductor/ferromagnet bilayer, vortex–antivortex chains, time-dependent Ginzburg–Landau equation

1. Introduction

Superconductivity and ferromagnetism are considered to be two irreconcilable properties, so their coexistence is very unlikely in bulk materials [1–3]. But it can be the realization of the coexistence in finite-geometry superconductor/ferromagnet (SC/FM) structures [2]. The interplay between superconductivity and ferromagnetism has attracted wide attention in the past few decades [4–7]. Indeed, the systems made of FM and SC films are extremely important for technological applications. Some recent reports on such hybrid systems mainly focused on proximity effects [2, 6, 7], magnetic domain walls [3, 8–11], critical temperature shift [12–15], arrays of magnetic dots [16, 17], magnetic dipoles [4, 18], and so on. Although many experiments and simulations have been carried out on its macroscopic properties, the pinning mechanism of the vortices induced by the FM film is still unclear. The studies involving finite-size SC/FM were limited primarily to the problem of (anti)vortex evolution. As far as is currently known, most of the reported works are not adequate to describe the transport features of the SC film embedded in the inhomogeneous magnetic field. It is essential to examine the variation in the domain patterns and the corresponding vortex structures in SC/FM hybrids through simulations and experiments.

Recently, the phenomena that a Py/Nb bilayer can exhibit strongly asymmetric and bistable transport properties have been demonstrated experimentally [5]. Meanwhile, numerical simulations show that the asymmetric and bistable magnetotransport response of the bilayers can be explained by the inhomogeneous magnetic field of the FM film [19]. In addition, the response of the SC film to the inhomogeneous magnetic field induced by the FM film shows that a spontaneous channeled flux flow regime is realized in the dissipative branch of the bilayer, with alternating vortex and antivortex chains moving in the opposite directions in the superconducting layer [19, 20]. Enlightened by these works, we report a mesoscopic model capable of describing the evolution of the inhomogeneous magnetic field of ferromagnet and its effect on the vortex–antivortex (V–Av) dynamics. In this work, we study the dynamic behavior of vortex–antivortex chains in the SC film placed under a finite-size FM film.

The paper is organized as follows. In Sect. 2, we explain the derived two-dimensional time-dependent Ginzburg–Landau equation (TDGL) equations and the numerical method used in the calculations. In Sect. 3, we analyze the transport features of SC film under different conditions. Finally, conclusions are summarized in Sect. 4.

2. Methods

The order parameter and the local magnetic field can be determined by the two-dimensional time-dependent Ginzburg–Landau equation, which is expressed by

$$u\left(\frac{\partial}{\partial t}+\mathrm{i}\varphi\right)\psi=\left(1-|\psi|^2\right)\psi-(\mathrm{i}\nabla+\boldsymbol{A})^2\psi, \tag{1}$$

$$\sigma\left(\frac{\partial \boldsymbol{A}}{\partial t}+\nabla\varphi\right)=\frac{1}{2\mathrm{i}}\kappa\left(\psi^*\nabla\psi-\psi\nabla\psi^*\right)$$

$$-|\psi|^2\boldsymbol{A}-\nabla\times\nabla\times\boldsymbol{A}. \tag{2}$$

The coefficient $u = 5.79$ controls the relaxation of the complex order parameter ψ, $|\psi|^2$ represents the electronic density of Cooper pairs, φ is the electrostatic potential, $\boldsymbol{A}$ denotes the vector potential, σ is the normal-state conductivity, $\kappa = \lambda/\xi$ is the GL parameter, $\lambda = \sqrt{m_s c^2\beta/(4\pi e_s^2|\alpha|)}$ is the magnetic field penetration depth (m_s is the Cooper pair mass and e_s is the effective charge of a Cooper pair), and ξ is the coherence length. All physical quantities are measured in dimensionless units. The superconducting order parameter ψ is in units of $\psi_0 = \sqrt{-\alpha/\beta}$ (α and β are the Ginzburg–Landau coefficients [4]), the distances are in units of the coherence length $\xi = \hbar/\sqrt{2m_s|\alpha|}$ ($\hbar$ is the Planck constant), the time is measured in units of the Ginzburg–Landau relaxation time $\tau_{\mathrm{GL}} = \pi\hbar/(8k_{\mathrm{B}}T_c)$($k_{\mathrm{B}}$ is the Boltzmann constant and T_c is the critical temperature), the vector potential $\boldsymbol{A}$ is in units of $A_0 = \sqrt{2}\kappa H_c\xi$ (H_c is the thermodynamically critical field). The usual isolator–superconductor boundary condition for the order parameter is given by

$$\boldsymbol{n}\cdot(-\mathrm{i}\nabla-\boldsymbol{A})\,\psi|_{\mathrm{boundary}}=0, \tag{3}$$

where $\boldsymbol{n}$ is the outward normal unit to the surface. The density of the superconducting current is given by

$$\boldsymbol{J_s}=\mathrm{Im}\left(\psi^*\nabla\psi-\psi\nabla\psi^*\right)|\psi|^2\boldsymbol{A}, \tag{4}$$

where Im denotes the imaginary part of the complex parameter. The driving current $\boldsymbol{j} = (0, j, 0)$ is introduced via the boundary condition for the vector potential in the x-direction, $\nabla\times\boldsymbol{A}|_z(x = 0, L) = H \pm H_j$, where $H_j = 2\pi j/c$ is the magnetic field by the driving current $\boldsymbol{j}$. The applied current density is scaled with $j_0 = \sigma\hbar/(2e\tau_{\mathrm{GL}}\xi)$. From the vector potential, it is possible to obtain the voltage using the expression $V = \frac{\partial}{\partial t}\int \mathrm{d}l\boldsymbol{A}$.

The local magnetic field $\boldsymbol{B} = \nabla\times\boldsymbol{A}$ is in units of $H_{c2} = \sqrt{2}\kappa H_c$. The effect of the ferromagnetic film on the SC film enters through the vector potential $\boldsymbol{A}$. The boundary condition is $\nabla\times\boldsymbol{A}|_{\mathrm{boundary}} = H$. The applied inhomogeneous magnetic field provided by ferromagnet is $\boldsymbol{H} = (0, B_z)$, given by [20]

$$B_z(x)=\frac{4\pi m\cosh\left(\frac{\pi a}{l}\right)}{l}\,\frac{\sin\left(\frac{\pi x}{l}\right)}{\sin^2\left(\frac{\pi x}{l}\right)+\sinh^2\left(\frac{\pi a}{l}\right)}, \tag{5}$$

where a is the distance from the upper face of the FM to the lower surface of SC, and m is the magnetization of ferromagnet and is in units of $m_0 = \Phi_0/(4\pi\lambda)$ (Φ_0 is the quantum of magnetic flux), l is the fixed width of the domain structure of the ferromagnet, and $l = 3\xi$. To simulate an infinite-length strip, we apply periodic boundary conditions in the y-direction.

The magnetization of the SC film is defined as $M = \frac{1}{4\pi}(\langle B\rangle - H)$ (here, $\langle B\rangle$ is the magnetic induction averaged over the superconductor film). The zero-scalar potential gauge is adopted $\varphi = 0$ at all times and positions. Our simulations have been carried out using $\sigma = 1$ and $\kappa = 1$. The initial conditions are $|\psi|^2 = 1$, corresponding to the whole simulation process.

3. Results and discussion

The thickness of the SC film is assumed to be sufficiently small compared with the London penetration depth (i.e., $d_s \ll \lambda$). For the convenience of computation, we perform 2D simulations by the finite element method [21]. Respective properties of different materials can be inhibited by intense interaction in hybrid systems consisting of materials with different or incompatible nature [22]. Based on this, a thin insulator film between SC and FM films is used to prevent the mutual suppression of superconductivity and ferromagnetism from happening. After that, the SC and FM films can only interact by ferromagnetic stray field and superconductor magnetization. So we only consider the coupling due to an inhomogeneous magnetic field. The thickness of the thin insulator film between SC and FM films is $a = 1\xi$ (see Fig. 1). In this work, we considered

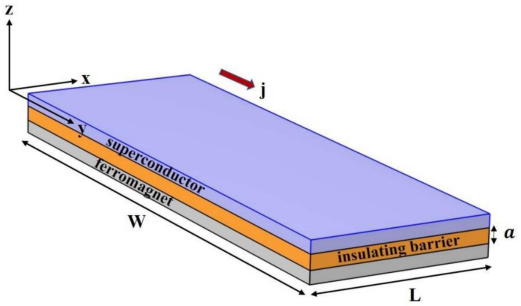

Fig. 1. Schematic view of the studied system — the SC/FM hybrid bilayer. Here, a is the thickness of the insulating barrier between SC and FM films.

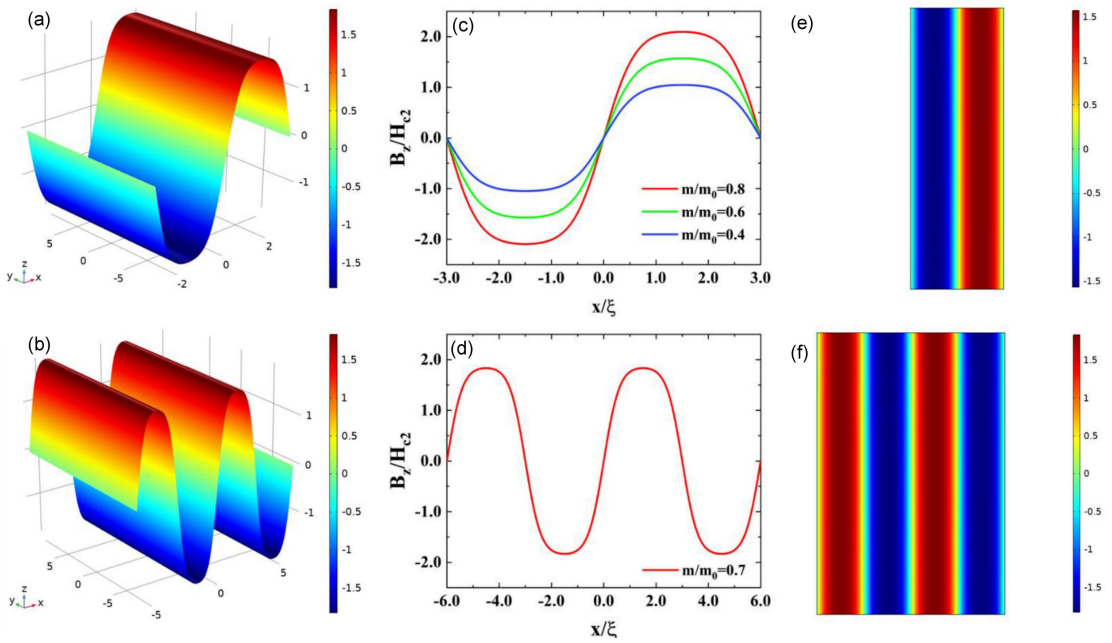

Fig. 2. (a) and (d) show z-component of the inhomogeneous magnetic field profile induced by the FM film; (b) and (e) — distribution of the inhomogeneous magnetic field induced by the FM film; (c) and (f) — chromatic scale plot of the inhomogeneous magnetic field acting on the SC film.

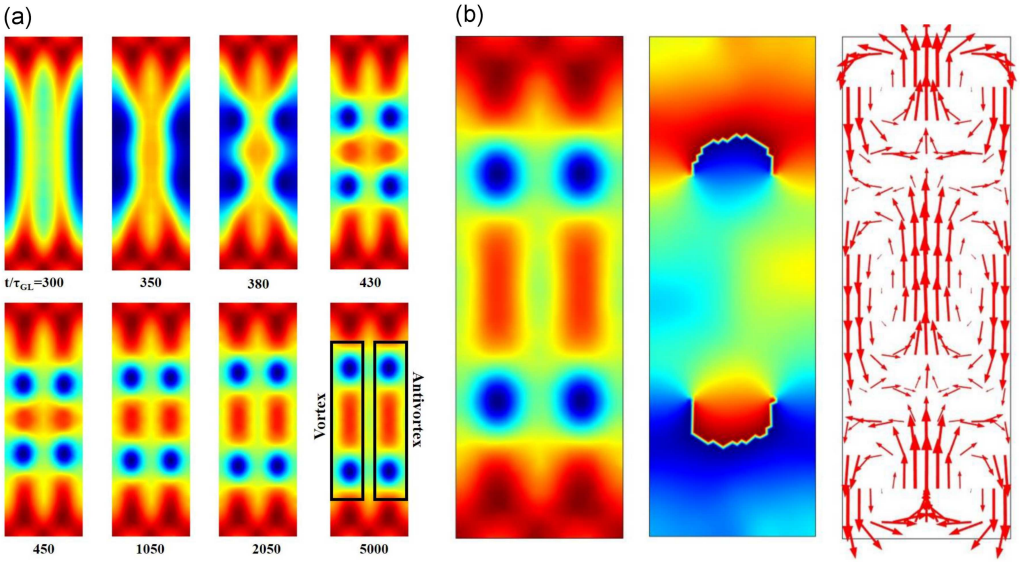

Fig. 3. (a) Nucleating process of V–Av pairs at $m/m_0 = 0.530$ for $j/j_0 = 0$. (b) Distributions of (anti) vortices, antiphase, and the superconducting current at $m/m_0 = 0.530$ for $j/j_0 = 0$.

a bilayer structure of size $W = 18\xi$ and $L = 6\xi$ (Fig. 2a–c) and a bilayer structure of size $W = 18\xi$ and $L = 12\xi$ (Fig. 2d–f). Figure 2 shows the distribution of the inhomogeneous magnetic field profile $B_z(x)$ induced by the FM film. The increasing magnetization of ferromagnet m increases the level of inhomogeneity of the magnetic field. Note that $B_z(x)$ is an odd function of x, which indicates that the spatial distribution of the inhomogeneous magnetic field is anti-symmetric. The maximum value of $B_z(x)$ can be reached at the center of the domain.

We first considered the bilayer structure of size $W = 18\xi$ and $L = 6\xi$. To show the specific nucleating process of V–Av pairs in the SC film, we plotted V–Av pairs configurations versus time t/τ_{GL} at $m/m_0 = 0.530$ for $j/j_0 = 0$ (see Fig. 3). When the external magnetic field is strong enough, the total superconducting current of SC film becomes higher than the depairing current, which lowers the surface barrier for the entry of V–Av pairs [23]. From the distribution of phase and the superconducting current (see Fig. 3b), the V–Av pairs appear

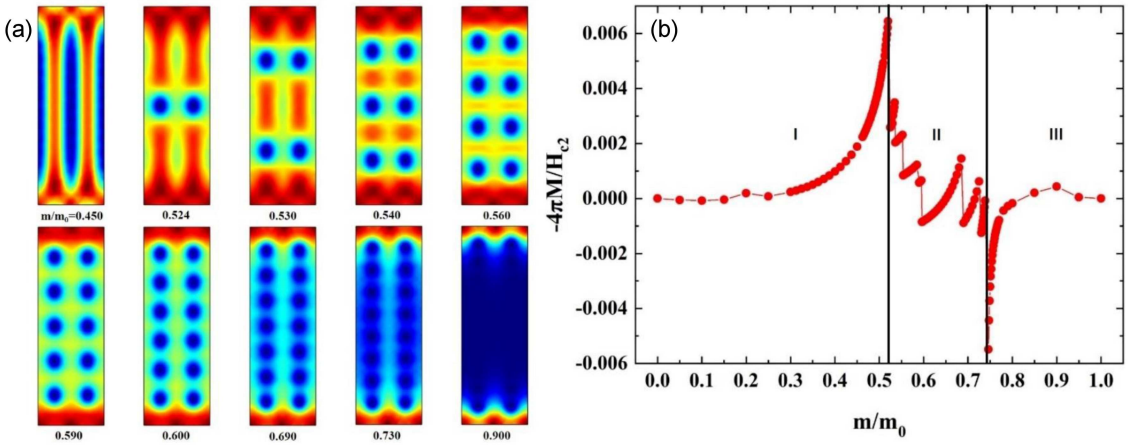

Fig. 4. (a) V–Av pairs configurations at $m/m_0 = 0.450$, $m/m_0 = 0.524$, $m/m_0 = 0.530$, $m/m_0 = 0.540$, $m/m_0 = 0.560$, $m/m_0 = 0.590$, $m/m_0 = 0.600$, $m/m_0 = 0.690$, $m/m_0 = 0.730$, and $m/m_0 = 0.900$ for $j/j_0 = 0$. (b) Magnetization as a function of the inhomogeneous magnetic field for different values of m.

symmetrically in both the left and right domains. The phenomenon is in agreement with what is found in the generation of (anti)vortices under the magnetic field induced by FM domains of the opposite polarity [24].

Figure 4 shows the nucleation of the V–AV pairs and magnetization for different m when $j/j_0 = 0$. The magnetization curve is divided into three types of regions. The I region ($< m/m_0 < 0.524$) shows the Meissner state. But only up to the first penetration field at $m/m_0 = 0.524$, the appearance of (anti)vortices makes the magnetization curve reach the maximum peak. The II region ($0.524 < m/m_0 < 0.730$) shows that the number and the rate of nucleation of the V–Av pairs increase with the increasing magnetization of ferromagnet m (see Fig. 4a). When the V–Av pairs enter the SC film, $M(m)$ decreases in a skip style [25, 26]. It consists of a set of steps, and each step corresponds to a fixed number of (anti)vortices in the channels. There are the same number of vortices and antivortices in each step since the total magnetic flux in the SC film is zero. The III region ($0.730 < m/m_0 < 1.00$) shows that the increasing magnetization of ferromagnet causes V–Av pairs to vanish. At present, the SC film makes a transition to the normal state.

As shown in Fig. 5, we investigate the effect of the magnetization of ferromagnet m on the dynamics of kinematic V–Av chains when the driving current $\boldsymbol{j}$ is applied along the y-direction of the SC film. The V–Av chains begin moving when $m/m_0 = 0.626$ and $j/j_0 = 0.008$, which indicates that the stationary flux motion mechanism has been established (Fig. 5a). The transport properties are coherent with the experimental results reported in [5]. Here, vortex chains move from top to bottom, and antivortex chains move from bottom to top. The forces of condition acting on the (anti)vortices in the SC film could be complex [18, 27, 28]. The vortices and antivortices enter the SC film with an inhomogeneous magnetic field and no driving current. When the magnetic force and the interaction between the vortices and antivortices are in equilibrium, the V–Av pairs are located at the center of the domains of the SC film. Once the driving current is applied, several forces work together to make the V–Av chains move along the y-direction, including the Lorentz force associated with the driving current, the magnetic force, which is generated by the inhomogeneous magnetic field, and the interaction between the vortices and antivortices. The frequency of periodic oscillations of the magnetization and superconducting current is adjusted by the inhomogeneous magnetic field (Fig. 5b–d). The frequency increases with the increasing magnetization of ferromagnet m. In order to facilitate the observation of the effect of the inhomogeneous magnetic field on the motion of V–Av chains, we plotted (see Fig. 5d) the periodic oscillations of magnetization with $m/m_0 = 0.660$ and $j/j_0 = 0.008$. The vortices and antivortices are pinned at the bottom of the SC film, which leads to the minimum (see inset 2) and maximum (see inset 4) of $M(t)$ curve. Consequently, the periodic motion of the V–Av chains is responsible for the magnetization oscillations in the SC film.

Figure 6a shows the I–V characteristics for the different values of magnetization of ferromagnet m. Because the order parameter of the system under the inhomogeneous magnetic field is suppressed, the critical current decreases with the increasing magnetization of the ferromagnet during the transition from the fully superconducting state to the resistive state. The obtained results are confirmed by the generally recognized properties of superconductors [16, 29]. Above the critical current, the SC film goes into the resistive state. We also calculated (see Fig. 6b and c) magnetization and superconducting current versus time t/τ_{GL} characteristics at $m/m_0 = 0.700$. When the driving current

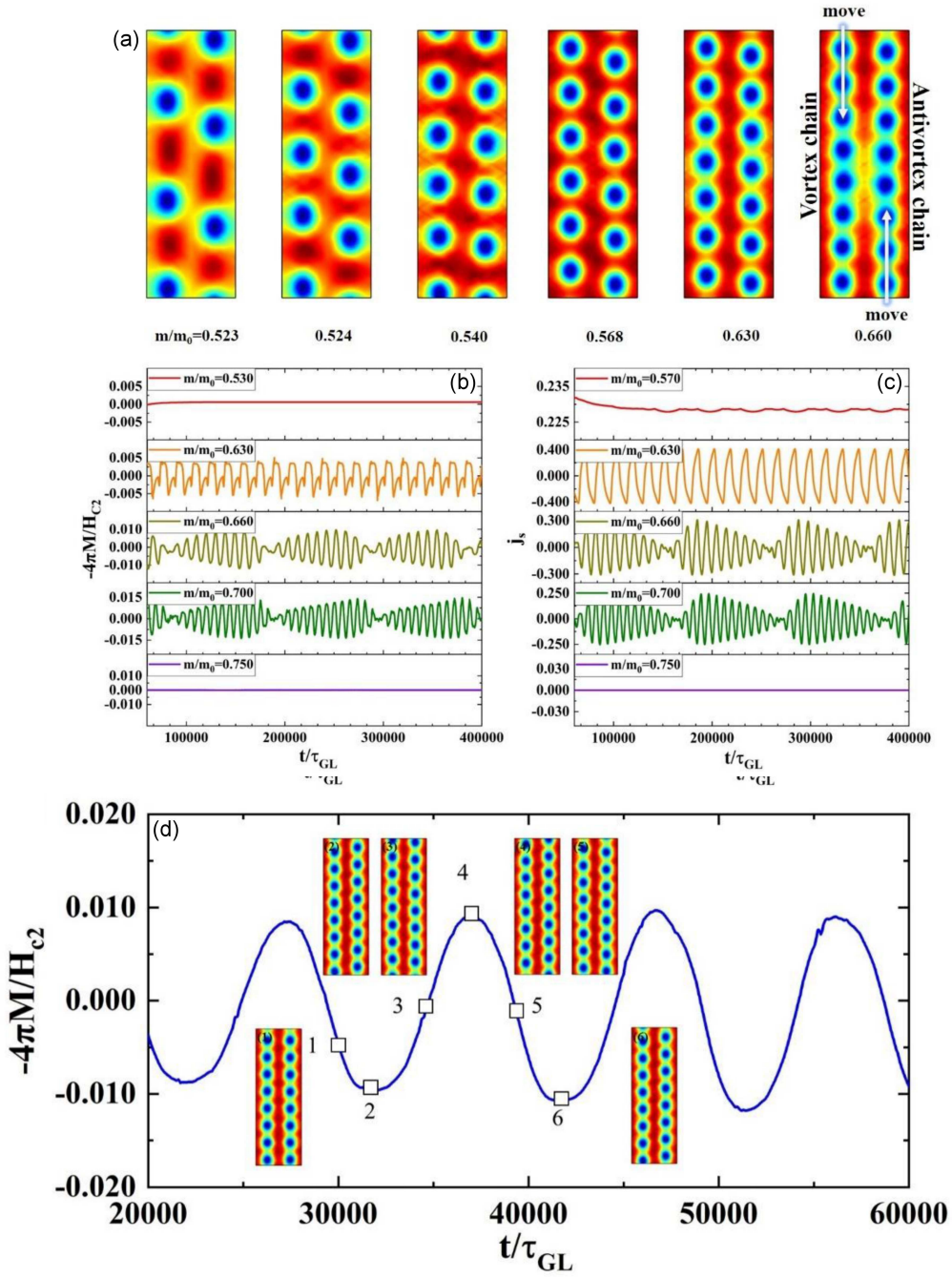

Fig. 5. (a) V–Av chains configurations at $m/m_0 = 0.523$, $m/m_0 = 0.524$, $m/m_0 = 0.540$, $m/m_0 = 0.568$, $m/m_0 = 0.630$, and $m/m_0 = 0.660$ for $j/j_0 = 0.008$. (b) Magnetization versus time characteristics of the SC film at $m/m_0 = 0.530$, $m/m_0 = 0.630$, $m/m_0 = 0.660$, $m/m_0 = 0.700$, and $m/m_0 = 0.750$ for $j/j_0 = 0.008$. (c) Superconducting current j_s versus time characteristics of the SC film at $m/m_0 = 0.570$, $m/m_0 = 0.630$, $m/m_0 = 0.660$, $m/m_0 = 0.700$, and $m/m_0 = 0.750$ for $j/j_0 = 0.008$. (d) Magnetization versus time characteristics of the SC film at $m/m_0 = 0.660$ for $j/j_0 = 0.008$.

increases, the rate of the nucleation (annihilation) process increases. The velocity of the motion of the V–Av chains increases with the increasing driving current, which means that the flux–flow resistance in the SC film decreases. A conclusion could be obtained that the frequency of periodic oscillations of the magnetization and superconducting current is adjusted by the driving current.

In order to further understand the dynamics behavior, we presented the movement of V–Av chains in the bilayer structure with sizes $W = 18\xi$ and $L = 12\xi$. As shown in Fig. 7, V–Av chains in the middle part remain stationary, while V–Av chains on either side of the SC film move alternately in the opposite directions at $m/m_0 = 0.700$ for $j/j_0 = 0.008$ (the arrows represent the direction of motion).

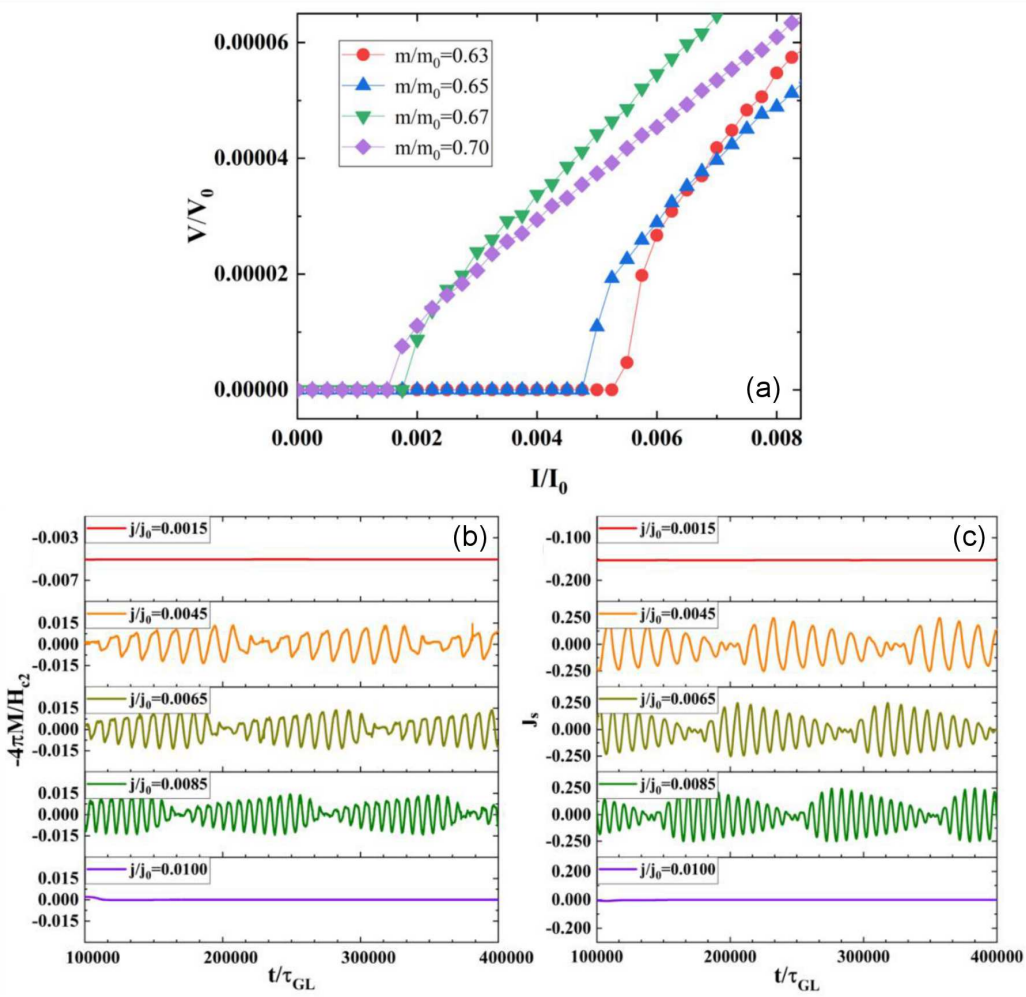

Fig. 6. (a) Time-averaged voltage as a function of the applied current for several values of magnetic fields. (b) Magnetization M and (c) superconducting current j_s versus time characteristics of the sample at $j/j_0 = 0.0015$, $j/j_0 = 0.0045$, $j/j_0 = 0.0065$, $j/j_0 = 0.0085$, and $j/j_0 = 0.0100$ for $m/m_0 = 0.700$.

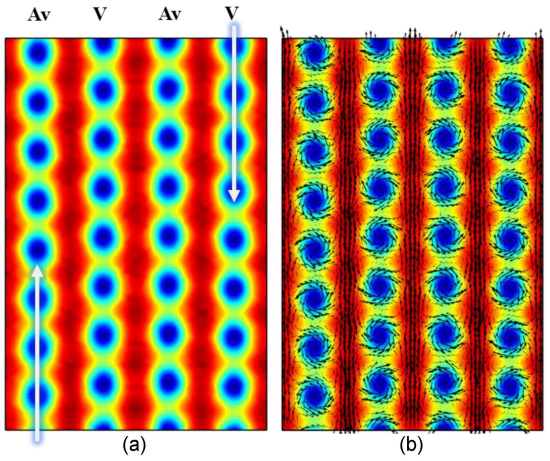

Fig. 7. (a) The movement of V–Av chains in the bilayer structure with sizes $W = 18\xi$ and $L = 12\xi$. The arrows represent the direction of motion at $m/m_0 = 0.700$ for $j/j_0 = 0.008$. V–Av chains in the middle remain stationary. (b) Distribution of superconducting current in the SC film.

By comparing Fig. 2c with Fig. 2f, we could conclude that the direction of the inhomogeneous magnetic fields of the FM film acting on the SC film determines the direction of the motion of the V–Av chains. Figure 8 shows the magnetization and superconducting current versus time characteristics in the SC film ($W = 18\xi$ and $L = 12\xi$) at different applied values of driving current and magnetization of ferromagnet. The same conclusion was obtained that the frequency of periodic oscillations of the magnetization and superconducting current is adjusted by the inhomogeneous magnetic field and the driving current.

4. Conclusions

In conclusion, we have reported numerical and analytical research on the transport properties of the SC film embedded in the inhomogeneous magnetic field of the FM film. Our results show that the coupling effect of superconductor/ferromagnet (SC/FM) structures manifests as the

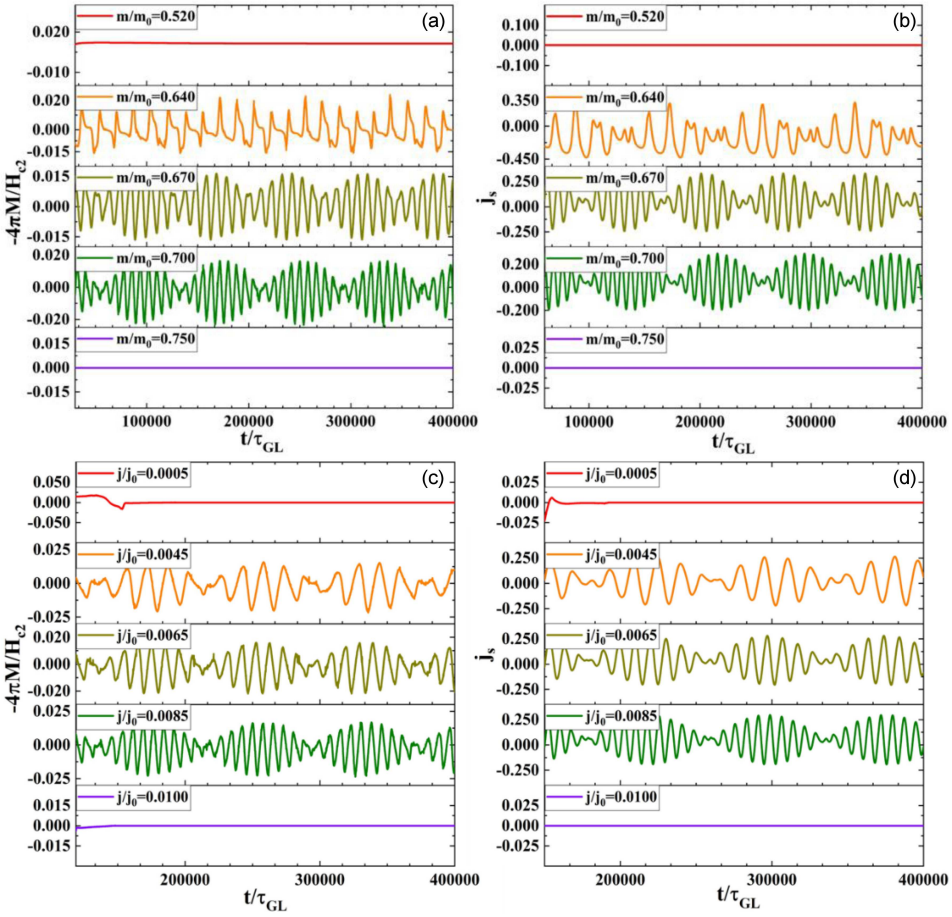

Fig. 8. (a) Magnetization M and (b) superconducting current j_s versus time characteristics of the SC film of size $W = 18\xi$ and $L = 12\xi$ at $m/m_0 = 0.520$, $m/m_0 = 0.640$, $m/m_0 = 0.670$, $m/m_0 = 0.700$, and $m/m_0 = 0.750$ for $j/j_0 = 0.008$. (c) Magnetization M and (d) superconducting current j_s versus time characteristics of the continuous SC film at $j/j_0 = 0.0005$, $j/j_0 = 0.0045$, $j/j_0 = 0.0065$, $j/j_0 = 0.0085$, and $j/j_0 = 0.0010$ for $m/m_0 = 0.700$.

vortex–antivortex (V–Av) pairs interaction. The coupling effect increases with the increasing level of inhomogeneity of the magnetic field. Moreover, the external driving current enhances this coupling effect, and the periodic motion of the V–Av chains leads to the periodic oscillations of the magnetization and superconducting current in the SC film. The frequency of oscillations is adjusted by the inhomogeneous magnetic field and the external driving current. Our results will be conducive to explaining the dissipative mechanism of V–Av dynamics and provide useful information for devices based on SC/FM heterostructures, such as superconducting quantum interference devices and superconducting memory devices.

Acknowledgments

This work was supported by the National Natural Science Foundation of China (Grants Nos. 12174246, 61875119) and the Science and Technology Commission of Shanghai Municipality (Grant No. 21010501300).

References

[1] A.Y. Aladyshkin, A.V. Silhanek, W. Gillijns, V.V. Moshchalkov, *Supercond. Sci. Tech.* **22**, 053001 (2009).

[2] A.I. Buzdin, *Rev. Mod. Phys.* **77**, 935 (2005).

[3] Z. Jing, H. Yong, Y.-H. Zhou, *Supercond. Sci. Tech* **27**, 105005 (2014).

[4] L. Peng, C. Cai, Y. Zhu, L. Sang, *J. Low Temp. Phys.* **197**, 402 (2019).

[5] G. Carapella, V. Granata, F. Russo, G. Costabile, *Appl. Phys. Lett.* **94**, 242504 (2009).

[6] S. Mironov, A.S. Mel'nikov, A. Buzdin, *Appl. Phys. Lett.* **113**, 022601 (2018).

[7] A.F. Volkov, F.S. Bergeret, K.B. Efetov, *Phys. Rev. B* **99**, 144506 (2019).

[8] M. Iavarone, S.A. Moore, J. Fedor, V. Novosad, J.A. Pearson, G. Karapetrov, *J. Supercond. Nov. Magn.* **28**, 1107 (2015).

[9] F. Aikebaier, P. Virtanen, T. Heikkilä, *Phys. Rev. B* **99**, 104504 (2019).

[10] R. Laiho, E. Lähderanta, E.B. Sonin, K.B. Traito, *Phys. Rev. B* **67**, 144522 (2003).

[11] M.Z. Cieplak, Z. Adamus, M. Kończykowski, L.Y. Zhu, X.M. Cheng, C.L. Chien, *Phys. Rev. B* **87**, 014519 (2013).

[12] Y.V. Fominov, N.M. Chtchelkatchev, A.A. Golubov, *Phys. Rev. B* **66**, 014507 (2002).

[13] V.A. Tumanov, Y.N. Proshin, *J. Low Temp. Phys.* **185**, 460 (2016).

[14] I.C. Moraru, W.P. Pratt, Jr., N.O. Birge, *Phys. Rev. Lett.* **96**, 037004 (2006).

[15] C.-Y. You, Y.B. Bazaliy, J.Y. Gu, S.J. Oh, L.M. Litvak, S.D. Bader, *Phys. Rev. B* **70**, 014505 (2004).

[16] G.R. Berdiyorov, M.V. Milošević, F.M. Peeters, *Phys. Rev. B* **80**, 214509 (2009).

[17] R.B.G. Kramer, A.V. Silhanek, W. Gillijns, V.V. Moshchalkov, *Phys. Rev. X* **1**, 021004 (2011).

[18] A.V. Kapra, V.R. Misko, D.Y. Vodolazov, F.M. Peeters, *Supercond. Sci. Tech.* **24**, 024014 (2011).

[19] G. Carapella, P. Sabatino, G. Costabile, *Phys. Rev. B* **81**, 054503 (2010).

[20] G.M. Maksimova, R.M. Ainbinder, D.Y. Vodolazov, *Phys. Rev. B* **78**, 224505 (2008).

[21] T.S. Alstrøm, M.P. Sřrensen, N.F. Pedersen, S. Madsen, *Acta. Appl. Math.* **63**, 115 (2011).

[22] I.F. Lyuksyutov, V.L. Pokrovsky, *Adv. Phys.* **54**, 67 (2005).

[23] A.V. Kapra, D.Y. Vodolazov, V.R. Misko, *Supercond. Sci. Tech.* **26**, 095010 (2013).

[24] V.S. Stolyarov, I.S. Veshchunov, S.Yu. Grebenchuk et al., *Sci. Adv.* **4**, eaat1061 (2018).

[25] P. Sabatino, G. Carapella, G. Costabile, *Supercond. Sci. Tech.* **24**, 125007 (2011).

[26] G. Carapella, P. Sabatino, M. Gombos, *Supercond. Sci. Tech.* **30**, 025018 (2017).

[27] G. Carapella, P. Sabatino, G. Costabile, *J. Appl. Phys.* **111**, 053912 (2012).

[28] G. Carapella, P. Sabatino, M. Gombos, *Physica C* **515**, 7 (2015).

[29] L. Peng, C. Cai, *J. Low Temp. Phys.* **183**, 371 (2016).